ELSEVIER

Surface Science 338 (1995) 261–278

surface science

Multilayer adsorption and desorption

S.H. Payne, H.J. Kreuzer *

Department of Physics, Dalhousie University, Halifax, N.S. B3H 3J5, Canada

Received 28 February 1995; accepted for publication 10 April 1995

Abstract

A multilayer lattice gas model for adsorption and desorption is formulated and solved using transfer matrix methods. Ramifications of nearest neighbor and next nearest neighbor interactions on equilibrium properties, on the growth modes, and on the desorption kinetics are studied in numerous examples. A variety of adsorbate structures and growth modes is obtained. Mass transfer between the layers can be induced, both under adsorption and desorption conditions.

Keywords: Adatoms; Adsorption kinetics; Growth; Metallic surfaces; Models of surface kinetics; Non-equilibrium thermodynamics and statistical mechanics

1. Introduction

Whereas adsorbates with mainly repulsive lateral interactions are generally restricted to the submonolayer regime, those with mainly attractive lateral interactions exhibit multilayer growth. Examples of the latter are most physisorbed systems such as rare gases and inert molecules on metals or insulators [1], but also strongly chemisorbed systems such as noble metals on transition metals and others [2]. But there are also systems where repulsive lateral interactions dominate in the submonolayer regime and attraction takes over in higher layers; alkalis on transition metals are an example. Although such systems have been studied experimentally for many years and are obviously of great interest and importance, little progress has been made on the theoretical side despite major advances in our understanding of adsorption and desorption in monolayer adsorbates. In this paper we will present a theory of multilayer adsorption and desorption based on a lattice gas.

Most of the applications of the lattice gas model to crystal growth have been concerned with calculating phase diagrams and critical properties, e.g. to establish the roughening transition [3–9]. Others, based on the solid-on-solid lattice gas model, have been to the study of detailed growth mechanisms [10,11]. The literature on the modeling of crystal growth is enormous, and is mainly concerned with phenomenological descriptions, see for example Refs. [12,13].

Our main interest is in the adsorption and desorption kinetics of the first few layers where effects of the adsorbate–substrate interaction are still at play. Our model of multilayer adsorption and desorption, to be presented in Section 2, is based on a lattice gas with nearest neighbor and next nearest neighbor interactions within and between the layers. Its equilibrium properties are calculated, essentially exactly,

* Corresponding author. Fax: +1 902 494 5191; E-mail: kreuzer@ac.dal.ca.

SSDI 0039-6028(95)00559-5

using the transfer matrix method. For the kinetics, described in Section 3, we assume that fast surface diffusion maintains the adsorbate in quasi-equilibrium. We present detailed results in Section 4, for bilayers, of the desorption spectra, heat of adsorption and growth modes.

2. Multilayer lattice gas

Most microscopic theories of adsorption and desorption are based on the lattice gas model. One assumes that the surface of a solid can be divided into two-dimensional cells, labelled i, for which one introduces microscopic variables $n_i = 1$ or 0, depending on whether cell i is occupied by an adsorbed gas particle or not. In its simplest form a lattice gas model is restricted to the submonolayer regime and to gas–solid systems in which the surface structure and the adsorption sites do not change as a function of coverage. In this paper we generalize this model to allow for the formation of multilayer adsorbates. We therefore introduce, in addition to n_i, second layer occupation numbers, $m_i = 0$ or 1 depending on whether the site i in the second layer is empty or occupied. Further layers are described similarly. To introduce the dynamics of the system one writes down a model Hamiltonian

$$\begin{aligned} H = {} & E_{s1}\sum_i n_i + E_{s2}\sum_i n_i m_i + \tfrac{1}{2}V_{11}\sum_{\text{n.n.}} n_i n_j \\ & + \tfrac{1}{2}V'_{11}\sum_{\text{n.n.n.}} n_i n_j + V_{12}\sum_{\text{n.n.}} n_i m_i n_j \\ & + \tfrac{1}{2}V_{22}\sum_{\text{n.n.}} n_i m_i n_j m_j + \tfrac{1}{2}V'_{22}\sum_{\text{n.n.n.}} n_i m_i n_j m_j \\ & + \ldots . \end{aligned} \tag{1}$$

Thus an isolated particle in the first layer contributes a single particle energy E_{s1}, and in the second layer it contributes E_{s2}. In this paper we assume on-top sites for the second layer although we can also deal with second layer adsorption sites in bridge or hollow sites, at least in one dimension. Returning to (1) we identify V_{11} (V'_{11}) and V_{22} (V'_{22}) as the lateral interactions between two particles in nearest neighbor (next-nearest neighbor) sites in the first and second layers, respectively. The interaction V_{12} is a trio interaction but because for $m_i = 1$ we must also have $n_i = 1$ we can also interpret V_{12} as a next-nearest neighbor interaction with one particle in the first layer and another in the second layer. The nearest neighbor interaction between a particle in the first layer and another one on top of it in the second layer is accounted for by E_{s2} which also contains the residual interaction with the substrate.

If we want to study adsorption–desorption kinetics, the number of particles in the adsorbate changes as a function of time and a proper identification of E_{si} is mandatory. Arguing that the lattice gas Hamiltonian should give the same Helmholtz free energy as a microscopic Hamiltonian (for non-interacting particles) one can show that the proper identification is given by [14]

$$E_{s1} = -V_0^{(1)} - k_B T \ln\left(q_3^{(1)} q_{\text{int}}^{(1)}\right) \tag{2}$$

and a similar expression for E_{s2}. Here $V_0^{(1)}$ is the (positive) binding energy of an isolated adparticle in the first layer. $V_0^{(2)}$ is the binding energy of a single adparticle in the second layer atop an isolated particle in the first layer, i.e. the difference $V_0^{(1)} - V_0^{(2)}$ accounts for the interaction between these particles and the shielding action of the first layer on the interaction of the second layer with the substrate.

$$q_3 = q_z q_{xy} \tag{3}$$

is a vibrational partition function with respect to the substrate with

$$q_z = \exp(h\nu_z/2k_B T)/\left[\exp(h\nu_z/k_B T) - 1\right] \tag{4}$$

its component for the motion perpendicular to the surface. Likewise, q_{xy} is the partition function for the motion parallel to the surface for which we will take a product of functions like (4). We have also made adjustment for the fact that the internal partition function for rotations and vibrations of an adsorbed molecule might be changed from its free gas phase value Q_{int} to q_{int}, if some of the internal degrees of freedom get frozen out or frustrated.

3. Adsorption–desorption kinetics

To model the adsorption–desorption kinetics we will assume that fast surface diffusion (fast on the time scale of adsorption and desorption) maintains the adsorbate in quasi-equilibrium. In such situations

the system at temperature T is completely characterized by the coverage, θ, with all correlation functions given by their equilibrium values. If non-equilibrium develops within the adsorbate during adsorption or desorption, these correlations deviate from their equilibrium values and a kinetic lattice gas model must be developed [14] to determine their time evolution.

The time rate of change of the coverage is due to an excess flux of molecules hitting the area, a_s, of an adsorption site and sticking with a probability $S(\theta,T)$, i.e. [15]

$$\frac{d\theta}{dt} = S(\theta,T)\, a_s \frac{\lambda}{h}(P-\bar{P}). \tag{5}$$

Here, $\lambda = h/(2\pi m k_B T)^{1/2}$ is the thermal wave length of a particle of mass m, P is the instantaneous pressure above the surface and $\bar{P}$ is the equilibrium pressure needed to maintain a coverage θ of atoms at the temperature T. Writing $\bar{P}$ in terms of the chemical potential of the adsorbate, μ_{ad}, we get for (5)

$$d\theta/dt = R_{ad} - R_{des}, \tag{6}$$

where the rates of adsorption and desorption are

$$R_{ad} = S(\theta,T)\, a_s \frac{\lambda}{h} P, \tag{7}$$

$$R_{des} = S(\theta,T)\, a_s \frac{k_B T}{h\lambda^2} Q_{int}\, e^{\mu_{ad}/k_B T}. \tag{8}$$

The chemical potential we split into a configurational term for a non-interacting lattice gas, $x(\theta)$, and a contribution, μ_i, due to lateral interactions

$$\mu_{ad}(\theta,T) = -V_0^{(1)} - k_B T \ln\left[q_3^{(1)} q_{int}^{(1)}\right] + k_B T \ln x(\theta) + \mu_i(\theta,T). \tag{9}$$

For an adsorbate restricted to two layers one can show that $x(\theta)$ is the positive root of

$$x^2(2-\theta)y + x(1-\theta) - \theta = 0, \tag{10}$$

with

$$y = \exp\left[\left(E_s^{(1)} x - E_s^{(2)}\right)/k_B T\right]. \tag{11}$$

For n layers we get an nth order polynomial instead of (10). With this we get for (8)

$$R_{des} = S(\theta,T)\, a_s \frac{k_B T}{h\lambda^2} \frac{Q_{int}\, x(\theta)}{q_3 q_{int}}\, e^{(-V_0^{(1)}+\mu_i)/k_B T}. \tag{12}$$

To make connection with the familiar monolayer lattice gas we note that $y \ll 1$ if the binding of the second layer is much weaker than that of the first. In this case we find for $\theta < 1$

$$x(\theta) = \theta/(1-\theta) + O(y), \tag{13}$$

which is the configurational partition function of an ideal monolayer lattice gas. The second layer contribution is

$$x(\theta) = (\theta-1)/y(2-\theta) + 1/(\theta-1) + O(y). \tag{14}$$

Since y is small the overpressure which is proportional to x must be large to force occupation of this layer.

To complete the theory we need (i) to specify the coverage dependence of the sticking coefficient and (ii) to calculate the lateral interaction part of the chemical potential, μ_i, of the adsorbate. The sticking coefficient is a measure for the efficiency of energy transfer in adsorption and desorption. As such it cannot be obtained from thermodynamic arguments but must be calculated from a microscopic theory or be postulated in a phenomenological approach, based on experimental evidence for a particular system or some simple arguments. For interacting systems it is generally both coverage and temperature dependent. To simplify matters we assume in this paper that sticking is independent of coverage as it is appropriate, e.g. for metals on metals.

We obtain the interaction part of the chemical potential, μ_i, by employing the transfer matrix method [16–22]. The transfer matrix is constructed for interactions between particles in a pair of adjacent rows, with periodicity of the interactions imposed for each row. As each adsorption site may contain 0,1 or 2 particles, corresponding to the states $|n_i m_i\rangle = |00\rangle$, $|10\rangle$ and $|11\rangle$, it is convenient to first recast the Hamiltonian (1) using the three-state basis with occupation numbers $n_i^{(a)} = n_i(1-m_i)$ and $n_i^{(b)} = n_i m_i$. The associated grand partition function, $\Xi(T, M, \mu)$, with μ the chemical potential of the particle reservoir over the surface, is then obtained as the leading eigenvalue, λ_1, of the transfer matrix, $\Xi = \lambda_1^M$, with the coverage given by

$$\theta = \frac{k_B T}{M} \left.\frac{\partial \ln \Xi}{\partial \mu}\right|_T. \tag{15}$$

In practice, it suffices to consider only the totally symmetric subblock of the transfer matrix for this calculation; θ is obtained from the corresponding eigenvector. Also, it is computationally expedient to specify coverage and temperature meshes and iterate to a consistent $\mu(\theta,T)$, from which all quantities of interest can be interpolated. Exact results can be obtained by this method for large enough M. For the results on a square lattice presented below, we have used $M=4$, which more than suffices to illustrate, accurately, the essential features.

The partial coverages for the two layers and the total coverage are defined in terms of the occupation numbers by

$$\theta_1 = N_s^{-1} \sum_i \langle n_i \rangle,$$

$$\theta_2 = N_s^{-1} \sum_i \langle m_i \rangle,$$

$$\theta = \theta_1 + \theta_2, \tag{16}$$

where N_s is the number of lattice sites in each layer, i.e. equal to M for the transfer matrix calculation.

4. Numerical examples

As we are primarily interested in exploring the influence of the binding and interaction energies on the adsorption and desorption characteristics of multilayer adsorbates, we shall reduce the number of parameters in the calculations by assuming, from now on, that the vibrational frequencies of isolated particles are the same in three directions and in both layers, i.e.

$$q_3^{(1)} = q_3^{(2)} \tag{17}$$

and that the gas phase and the adsorbate consist of atoms only, so that $Q_{\text{int}} = q_{\text{int}} = 1$. We now proceed in stages of classes of lateral interactions.

4.1. No lateral interactions

To establish a reference we start with an adsorbate in which lateral interactions are negligible. Fig. 1a shows temperature programmed desorption (TPD) rates, R_{des}, for a situation where the difference between the second layer binding energy and the first layer binding energy

$$\Delta V_0 = V_0^{(1)} - V_0^{(2)} \tag{18}$$

is a few percent of either. This results in TPD spectra with a slight peak shift to lower temperature for increasing initial coverage due to the prior desorption of the less strongly bound second layer, as shown in Fig. 1b which depicts the partial rates.

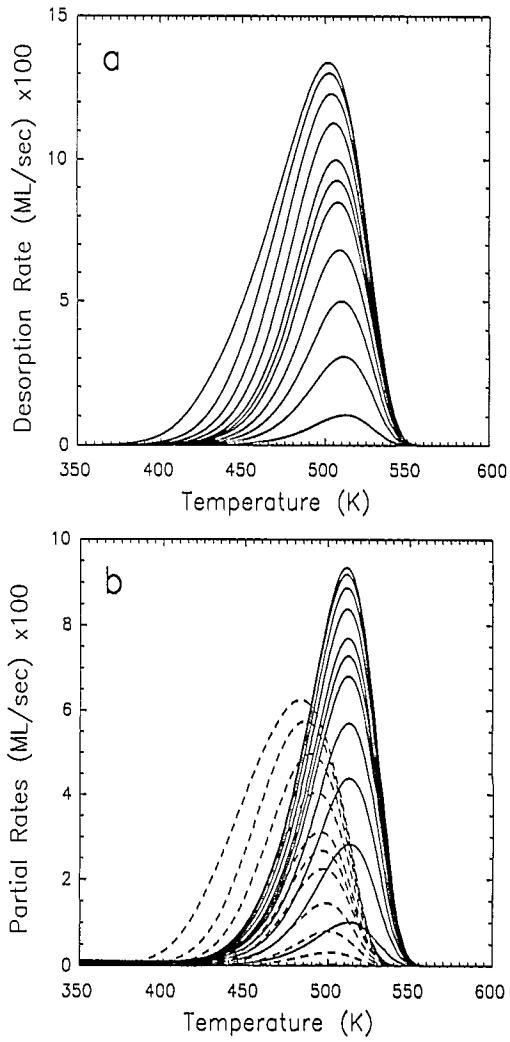

Fig. 1. (a) Total desorption rates in TPD (with heating rate $\alpha = 5$ K s^{-1}) for a system without lateral interactions. Parameters, fixed for all examples: $V_0^{(1)} = 14500$ K, $m = 28$ amu, $a_s = 10$ Å^2, $\nu_x = \nu_y = \nu_z = 5 \times 10^{11}$ s^{-1}. Binding difference $\Delta V_0 = 500$ K. Initial coverages: 0.1, 0.3, 0.5, 0.7, 0.9, 1.0, 1.1 .... 1.9. (b) Partial rates of first layer (solid) and second layer (dashed).

Increasing ΔV_0 will result in a splitting of the desorption peak as in Fig. 2a with the lower peak corresponding to desorption from the second layer, see Fig. 2b. Fig. 2c shows the partial coverages as a function of temperature. Of interest is the fact that, for initial coverages around one monolayer and before significant desorption occurs, particles are transferred from the first to the second layer as temperature increases. This happens because (i) the effective binding in the second layer is lower, and (ii) nearly all the sites in the second layer are now available for promotion of the first-layer particles. This transfer can be enhanced by interactions between the particles. Because the slopes of the partial coverages, $\theta_i(T)$, are proportional to the partial rates, a decrease in θ_1 implies a (positive) partial rate, $-\mathrm{d}\theta_1/\mathrm{d}t$, below 400 K, where the total rate is still zero (for initial coverages around a monolayer). The complementary partial rate from the second layer is thus negative (but not shown in Fig. 2b). Of course, only the total rate is observable and it is never negative. This results in the crossing of the first layer rate curves for initial coverages of order unity. Recall that we assumed that fast surface diffusion maintains the adsorbate in quasi-equilibrium so that the partial coverages remain at their equilibrium values, i.e. in the ratio (for a non-interacting adsorbate)

$$\theta_1/\theta_2 = 1 + 1/xy = 1 + x^{-1}\,\mathrm{e}^{\Delta V_0/k_\mathrm{B}T}, \qquad (19)$$

where $x = x(\theta)$ is given by (10). Note again the shift in the peak positions to lower temperature, for each layer, as the initial coverage is increased. This time it is not due to the overlapping desorption, as the second layer has essentially disappeared at the peak rates for the first layer. Nor is it to be interpreted as a typical manifestation of lateral repulsions, which are not present in this example. Rather, it is due to our choice of a constant sticking coefficient. This can be seen from the expression for the desorption rate (12) of a monolayer adsorbate maintained in quasi-equilibrium during desorption. In the absence of lateral interactions $\mu_i = 0$, $x(\theta)$ is given by (13) and the rate is first order, and will not show a peak shift in TPD, if $S(\theta) = S_0(1-\theta)$. For a non-interacting multilayer adsorbate the sticking coefficient should be

$$S(\theta) = S_1(1-\theta_1) + S_2\theta_1, \qquad (20)$$

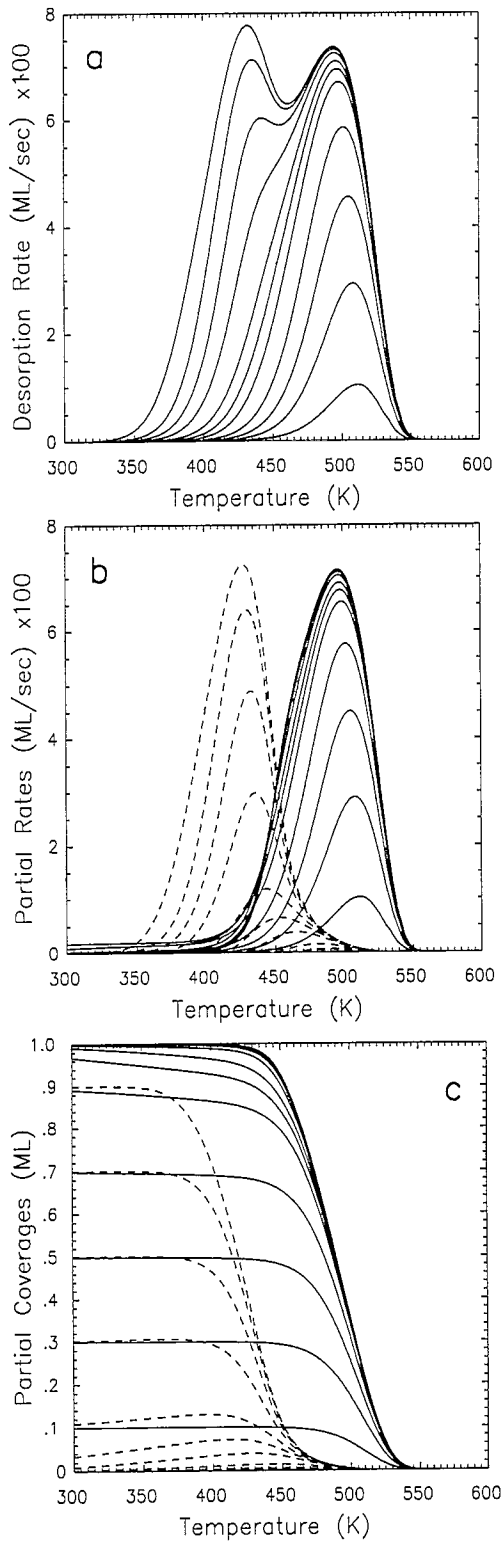

Fig. 2. Same as Fig. 1 but with $\Delta V_0 = 2000$ K; (c) partial coverages, corresponding to (b).

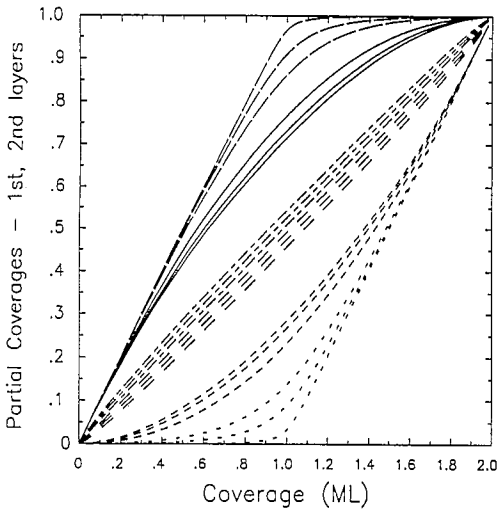

Fig. 3. Isothermal layer growth curves for temperatures spanning the desorption range. Top to bottom: θ_1 for Fig. 2 ($\Delta V_0 = 2000$ K, long dashed lines) with $T = 300$, 450, 600 K; θ_1 for Fig. 1 ($\Delta V_0 = 500$ K, solid) with $T = 300$, 450, 600 K; θ_1 for $\Delta V_0 = -2000$ K, short-long dashes) with $T = 650$, 500, 350 K. The remaining curves are θ_2 curves, in reverse order.

because sticking on the bare surface is controlled by the available number of sites, θ_1, and in the second layer by the number of occupied sites in the first. Thus if $S_1 = S_2$ we see that the denominators of (13) and (14), arising from the configurational entropy, are responsible for the observed shifts. Choosing $S_1 \neq S_2$ will *re*-adjust the relative peak heights and cause small shifts in their positions.

A further weakening in the second layer binding, i.e. ΔV_0 increasing, results in a larger splitting, ΔT, of the TPD peaks, which can be estimated from Redhead's formula $\Delta T \simeq \Delta V_0/30$ (for a heating rate of 5 K s^{-1} and a constant prefactor of 10^{13} s^{-1}). However, if the binding of the second layer is stronger than that of the first this leads to a stabilization of the first layer. As a result desorption from the two layers is almost simultaneous and the total rate is similar to that of Fig. 1a with the differences that

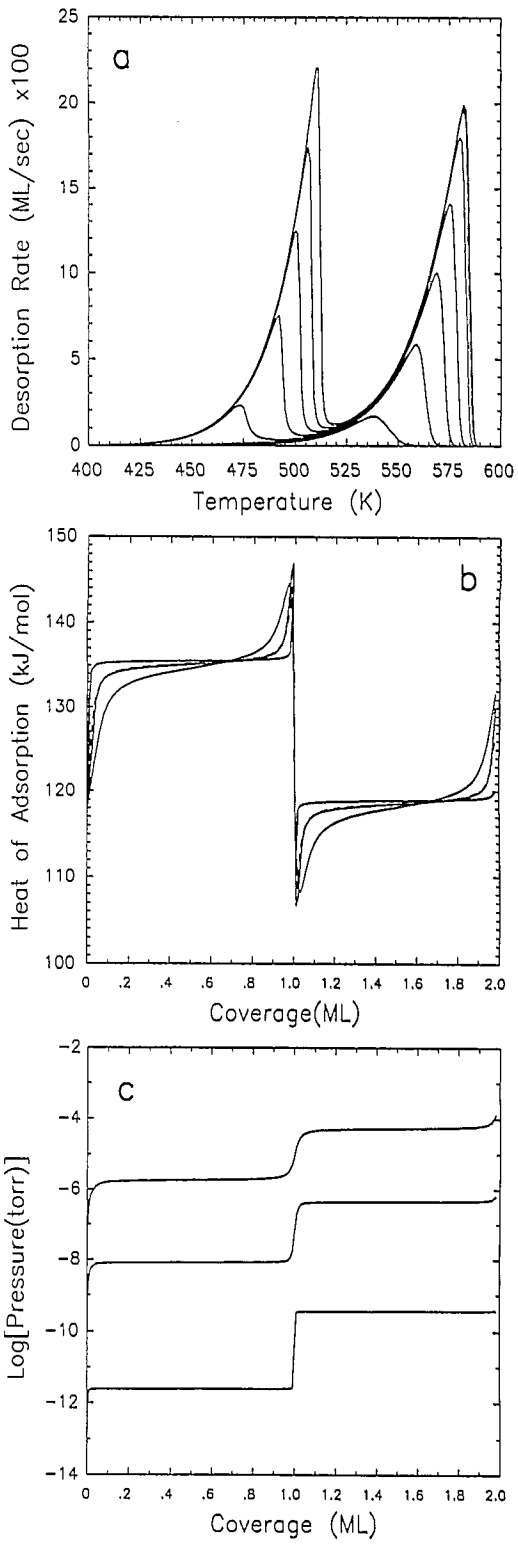

Fig. 4. Lateral attractions in both layers, $V_{11} = V_{22} = -1000$ K, $V_{12} = 0$ K, $\Delta V_0 = 2000$ K. Other parameters as in Fig. 1. (a) Total rates, initial coverages as in Fig. 1. (b) Isothermal heat of adsorption for $T = 400$, 500, 600 K (top to bottom at low θ). $T_c = 567$ K for independent layers. (c) Pressure isotherms for the same temperatures (bottom to top).

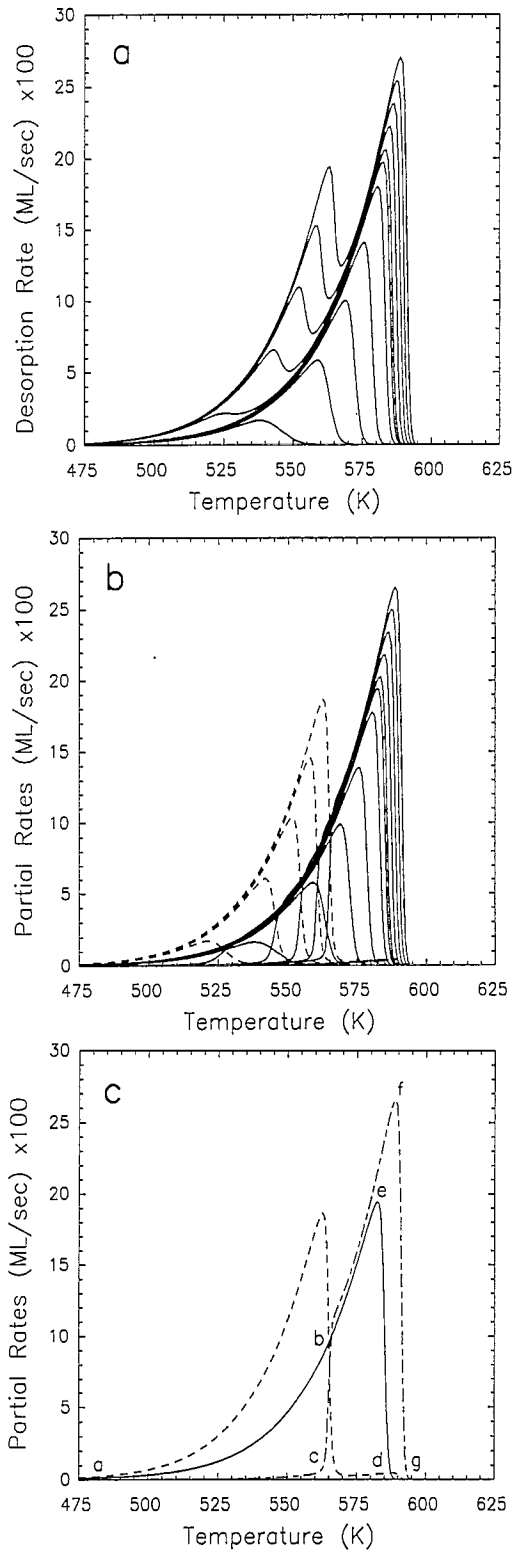

Fig. 5. As Fig. 4 but $\Delta V_0 = 500$ K. (a) Total rates and (b) partial rates. (c) Partial rate $-\mathrm{d}\theta_1/\mathrm{d}t$ for $\theta_0 = 1.0$ (solid line) and $\theta_0 = 1.9$ (long-short dashes), and $-\mathrm{d}\theta_2/\mathrm{d}t$ for $\theta_0 = 1.9$ (dashed).

(i) the spectra are narrower, (ii) the peak positions shift to higher temperatures for increasing initial coverage, and (iii) the trailing edges drop precipitously.

Fig. 3 displays the layer growth curves, i.e. isothermal partial coverages as a function of total coverage for the three cases. Whereas for the system of Fig. 1 there is a concurrent growth of both layers, the system of Fig. 2 tends towards layer-by-layer growth. Nevertheless, even here at high temperature holes necessarily develop in the first layer due to promotion of particles into the second layer. For the system with a stronger binding of the second layer there is dimer growth, i.e. more or less every first layer atom is topped by a second atom, $\langle n_i \rangle \simeq \langle m_i \rangle$.

4.2. Lateral attraction in two layers

Adsorbates capable of multilayer growth must have attractive interactions between the constituents once the binding to the substrate becomes negligible. In some adsorbates, such as rare gases on metals and noble metals on transition metals, attractive interactions already prevail in the submonolayer regime. In this section we will discuss such systems restricting ourselves to nearest neighbor interactions only.

We begin with a two-layer system in which the second layer is bound considerably weaker to the surface than the first, and the nearest neighbor interactions in the first and second layers are equal, $V_{11} = V_{22}$ (in magnitude about twice as much as the median desorption temperature), and $V_{12} = 0$ K. The TPD spectra, shown in Fig. 4a, exhibit two peaks indicating layer-by-layer desorption. Each peak has a common leading edge corresponding to desorption from a two-phase adsorbate. This is also illustrated by the isosteric heat of adsorption, per particle,

$$Q_{\mathrm{iso}}(\theta,T) = k_{\mathrm{B}}T^2 \left.\frac{\partial \ln \bar{P}}{\partial T}\right|_{\theta} \tag{21}$$

in Fig. 4b, derivable from sets of pressure isotherms, as shown in Fig. 4c. These show, for each layer, the

features typical of a monolayer lattice gas for strong nearest neighbor attraction, namely at low temperature a chemical potential constant with coverage, except outside the coexistence region where the chemical potential increases rapidly at the completion of the monolayer and, correspondingly, decreases at low coverage. Thus the sharp features at $\theta = 1$ reflect the strict layer-by-layer growth mode, i.e. $\theta_2 = 0$ for $\theta < 1$ and $\theta_1 = 1$ for $\theta > 1$. Although finite size effects ($M \times \infty$ lattice) are present here, the phase boundaries for the layers for $M \to \infty$ can be determined from the transfer matrix by a power law extrapolation on M [19]. These TPD spectra and heats of adsorption are reminiscent of experimental data for noble metals adsorbed on metal substrates, e.g. Cu [23] and *Au* [24] on *Mo*(110), *Ag* and *Au* on *Ru*(001) [25] and *Cu* on W(110) [26]. A detailed discussion of some of these systems will be given elsewhere [27].

In our next example, Fig. 5, we decrease ΔV_0 to that of Fig. 1 which shifts the second layer desorption peak onto the leading edge of the first layer. Their partial rates in Fig. 5b still show apparent independent desorption of the two layers with the first layer trailing the second at higher temperatures except for a small overlap. However, desorption from the first layer is now constrained by that of the second, resulting in an additional small shift of the first layer peak (additional to the overall shift due to zero order desorption) for initial coverages larger than one monolayer to higher temperatures, as compared to one monolayer. We illustrate this explicitly in Fig. 5c for initial coverages, $\theta_0 = 1.0$ and 1.9 ML. The presence of the second layer suppresses the desorption of the fraction of the first layer represented by the area under the '*curve*' abc. This amount of material will desorb instead at higher temperatures, and under the '*curve*' defg. This type of feature is commonly observed, e.g. for rare gases on metals [1]. For absorption of several layers the chemical potential will tend towards its bulk value which implies that the low temperature peak extends to higher rates and somewhat higher temperatures.

If we bind the second layer more strongly than the first but leave all other parameters as in Fig. 4 and Fig. 5 then for temperatures below critical the system will have two *co*-existing phases, i.e. a gas of vertical dimers and a condensed phase, with the heat of adsorption and also the chemical potential being constant as a function of coverage. TPD traces then show one common leading edge for both layers and desorption essentially taking place in pairs with one particle from the upper and then one from the lower layer. However, this does not imply that the desorption products are dimers because for the latter to form they must be stable in the gas phase at the chemical potential which is equal numerically to that of the adsorbate at the desorption temperature (and remaining coverage).

4.3. Lateral repulsion in first layer and attraction in higher layers

Some multilayer adsorbates show repulsive lateral interactions in the submonolayer regime which switches to attraction as a second layer builds up to allow for multilayer growth. Examples are alkalis and rare earth metals on transition metals which form '*ionic*' bonds with the surface. The formation of dipoles in the submonolayer regime also leads to repulsion which by simple reorientation can switch to attraction in the higher layers.

We choose the repulsion in the first layer to be equal in magnitude to the attraction in the second layer, $V_{11} = -V_{22} = 1000$ K. For this repulsion the first layer alone would desorb as two well separated peaks in TPD spectra with the separation in temperature being roughly 130 K for $\alpha = 5$ K s^{-1}. For $\Delta V_0 = 7000$ K, so large that the second layer peak overlaps with the low temperature peak of the first layer, we get the TPD spectra in Fig. 6a. Despite this apparent overlap there is still a more or less layer-by-layer desorption, with a small overlap of the partial rates just above a monolayer, as demonstrated in Fig. 6b where we plot the partial coverages as a function of the total coverage. An interesting feature also appears in the partial rates: because the second layer is still present in the temperature region where the first layer alone would have started to desorb, the latter will desorb initially with abnormally high rates as soon as the second layer is gone. This results in the low temperature spikes in the first layer partial rates in Fig. 6c. Subsequent desorption follows that of the first layer alone. For completeness we also give the heat of adsorption and equilibrium isotherms in Fig. 6d and Fig. 6e. The drop in the heat of

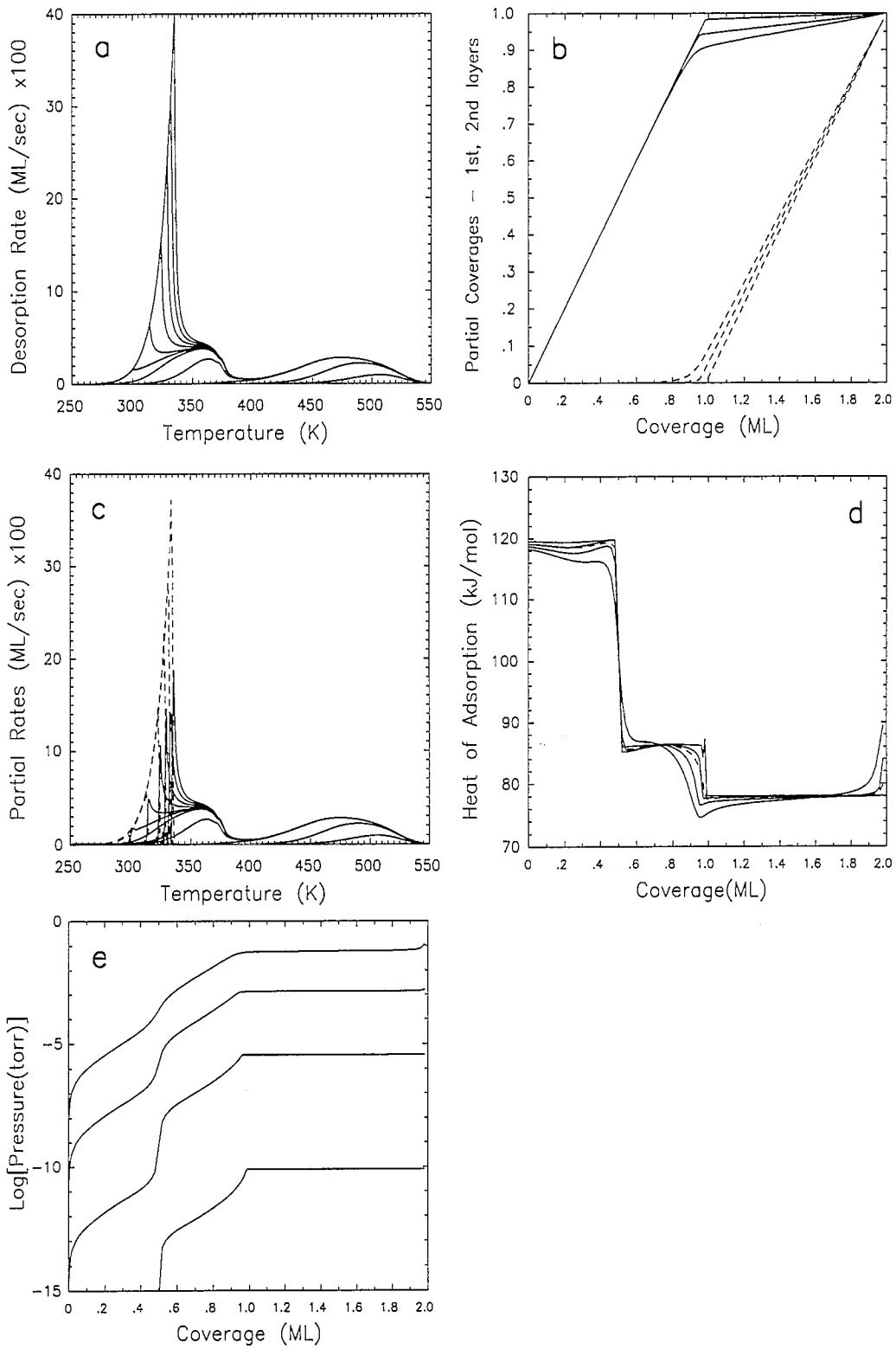

Fig. 6. Lateral repulsion in the first layer and attraction in the second, $V_{11} = -V_{22} = 1000$ K, $V_{12} = 0$ K, $\Delta V_0 = 7000$ K. Other parameters as in Fig. 1. (a) Total rates, initial coverages as in Fig. 1. (b) Growth curves, θ_1 (solid lines) for $T = 250$, 400, 550 K (top to bottom), and θ_2 (dashed) in reverse order. (c) Partial rates. (d) Isothermal heat of adsorption for $T = 250$, 350, 450, 550 K (top to bottom at low θ, solid curves). Dashed curve is the temperature averaged value. (e) Pressure isotherms for the same temperatures (bottom to top).

adsorption at $\theta = 1/2$, of magnitude $4V_{11}$, is due to the formation of a c(2 × 2) ordered structure arising from the nearest neighbor repulsion. Its onset is also signalled by the upturn of $Q(\theta,T)$ just below half a monolayer [21]. The features of this model system are qualitatively similar to those observed experimentally for *Li/Ru*(001) [28]; we will also present a detailed analysis of this system elsewhere [29].

If we decrease ΔV_0 the second layer desorption peak will be moved to higher temperatures and one can have the situation of Fig. 7a where the two peak structure of the first layer desorption of Fig. 6a is completely suppressed, as also shown in the partial rates of Fig. 7c. In contrast to Fig. 6 where approximate layer-by-layer growth and desorption occurred we now find that the second layer already starts to grow around $\theta \simeq 1/2$ and that for $\theta > 1.6$ the two layers go down together, as illustrated in Fig. 7b. The heat of adsorption is correspondingly more complicated, see Fig. 7d.

Provided the second layer attraction is strong enough, and ΔV_0 is small, or even negative, it is possible to recover the two-phase regime of a system of dimers alluded to in Section 4.1. We show Fig. 8

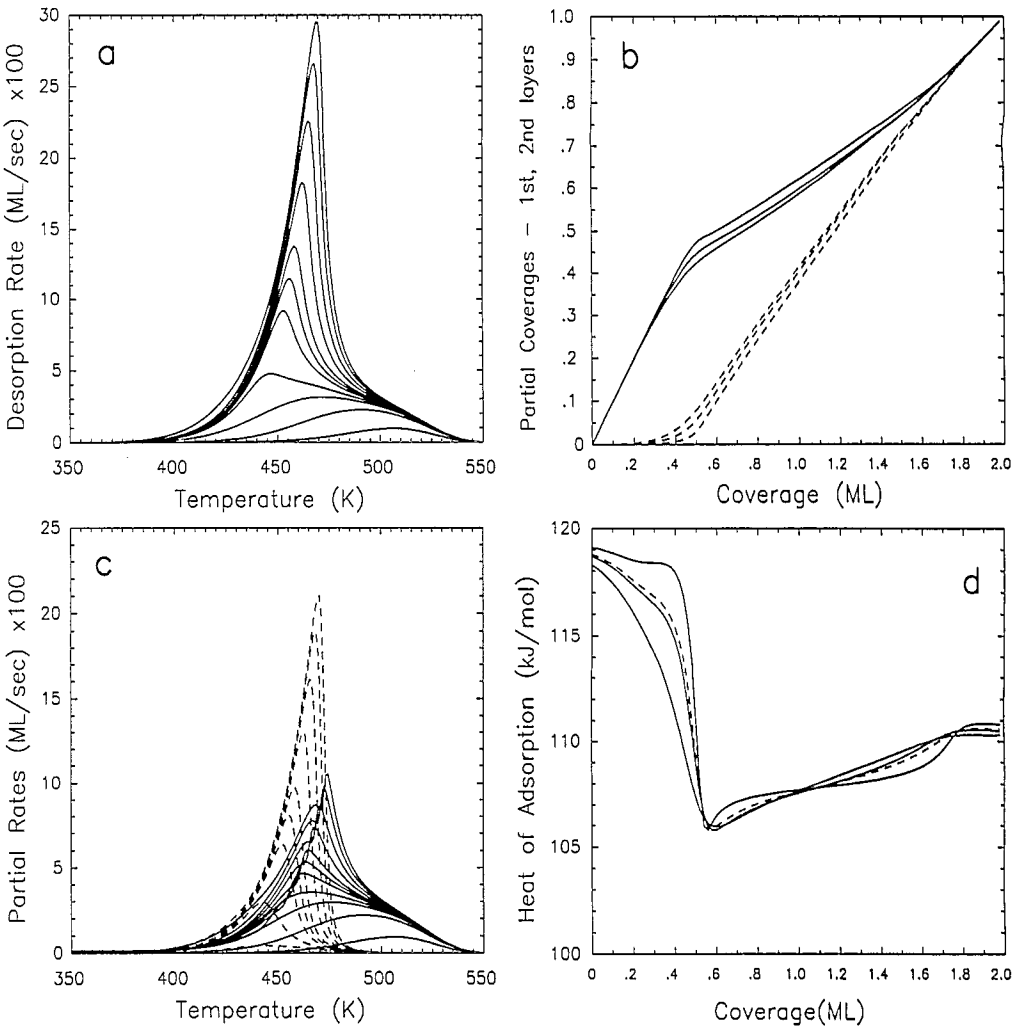

Fig. 7. Lateral repulsion in the first layer and attraction in the second, $V_{11} = -V_{22} = 1000$ K, $V_{12} = 0$ K, $\Delta V_0 = 2000$ K. Other parameters as in Fig. 1. (a) Total rates, initial coverages as in Fig. 1. (b) Growth curves, θ_1 (solid lines) for $T = 350$, 450, 550 K (top to bottom), and θ_2 (dashed) in reverse order. (c) Partial rates. (d) Isothermal heat of adsorption for $T = 350$, 450, 550 K (top to bottom at low θ, solid curves). Dashed curve is the temperature averaged value.

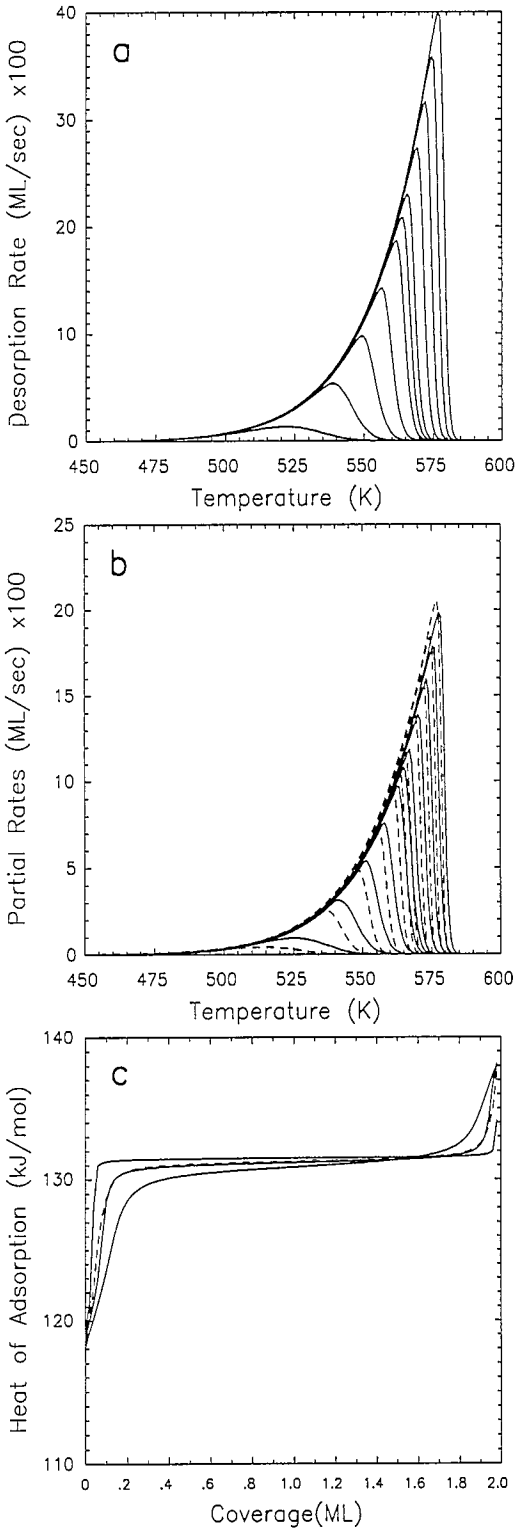

as an example. In the absence of an absolute coverage determination the desorption might be interpreted as being from the coexistence regime of a single layer. Essentially the same features are obtained for a range of interaction and binding energies.

We next look at a system, Fig. 9, with negligible interactions in the second layer and otherwise the same as in Fig. 7. Although the absence of the second layer attraction has eliminated the common leading edge, the second layer desorption still constrains the lower peak of the first layer desorption to higher temperatures but not as much as in Fig. 7c because the partial rate of the first layer in Fig. 9c still shows a two-peak structure, albeit compressed in comparison to a situation where a second layer could not form at all. The growth mode and heat of adsorption in Fig. 9b and Fig. 9d, respectively, are again quite complex but in some features reminiscent of Fig. 7. The overlap of the first and second layer desorption traces also manifests itself in the transfer of particles from the second layer down to the first around one monolayer total coverage as temperature increases, Fig. 9e, and this despite the repulsion in the first layer. For the system of Fig. 7 the transfer is in the opposite direction. The transfer is also transparent in the crossing of the isotherms in Fig. 9b around 0.7 monolayers. As neither the total desorption rate nor the (featureless) pressure isotherms signify this regime, other techniques must be employed to detect it, for instance work function measurements.

4.4. Lateral repulsion in first and second layers

Although we are not aware of systems in which two layers can exist with lateral interactions being strongly repulsive in both, we present two examples in Fig. 10 to show the complexity of such systems. If the repulsion is such that for desorption from either

Fig. 8. Lateral repulsion in the first layer and attraction in the second, $V_{11} = -0.5$ $V_{22} = 1000$ K, $V_{12} = 0$ K, $\Delta V_0 = -1000$ K. Other parameters as in Fig. 1. (a) Total rates, initial coverages as in Fig. 1. (b) Partial rates. (c) Isothermal heat of adsorption for $T = 400$, 500, 600 K (top to bottom at low θ, solid curves). Dashed curve is the temperature averaged value.

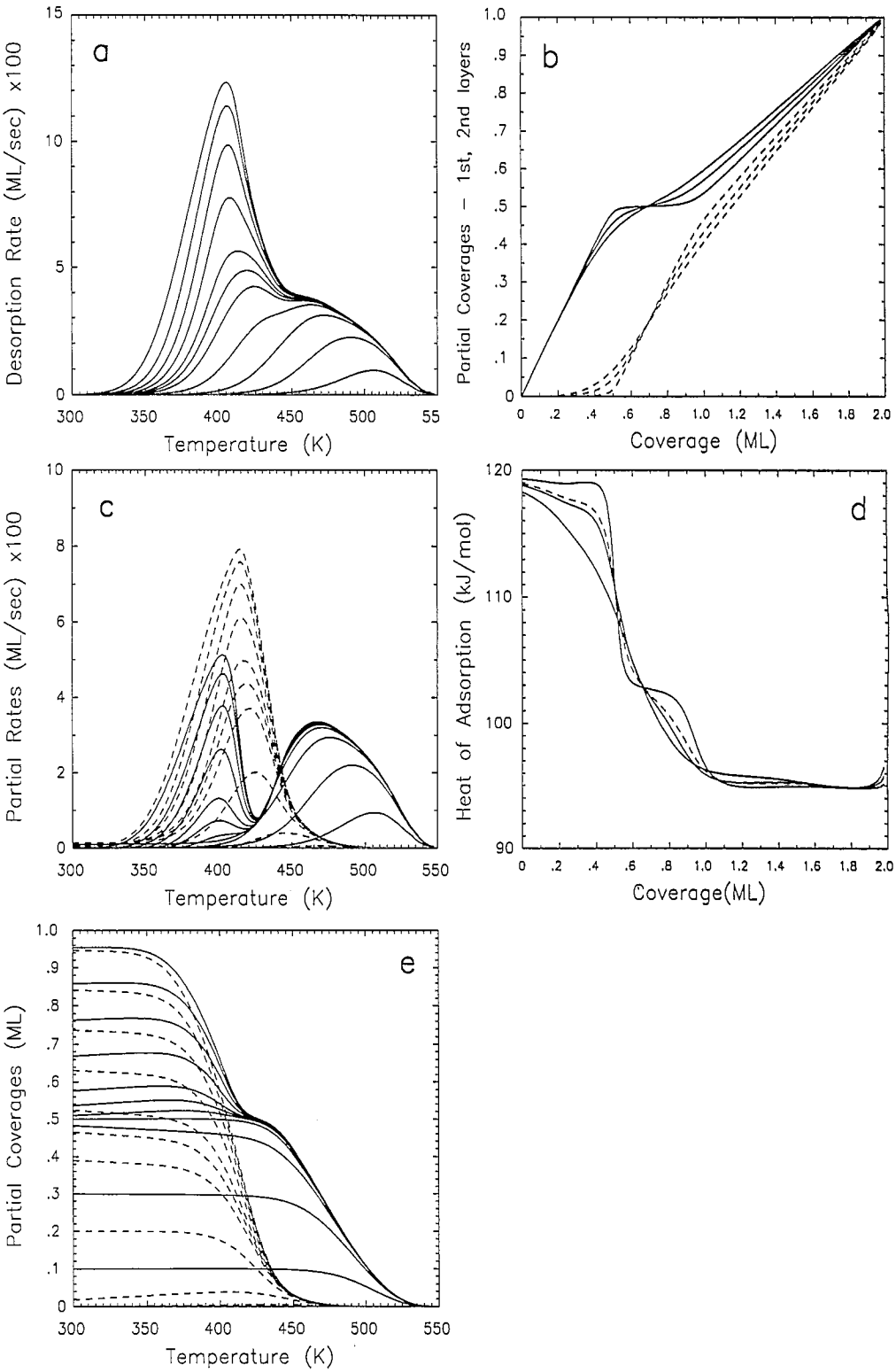

Fig. 9. Lateral repulsion in the first layer, $V_{11} = 1000$ K, and no interactions $V_{22} = V_{12} = 0$ K, $\Delta V_0 = 2000$ K. Other parameters as in Fig. 1. (a) Total rates, initial coverages as in Fig. 1. (b) Growth curves, θ_1 (solid lines) for $T = 300$, 425, 550 K (top to bottom at $\theta = 0.4$), and θ_2 (dashed) in reverse order. (c) Partial rates. (d) Isothermal heat of adsorption for $T = 300$, 425, 550 K (top to bottom at low θ, solid curves). Dashed curve is the temperature averaged value. (e) Partial coverages.

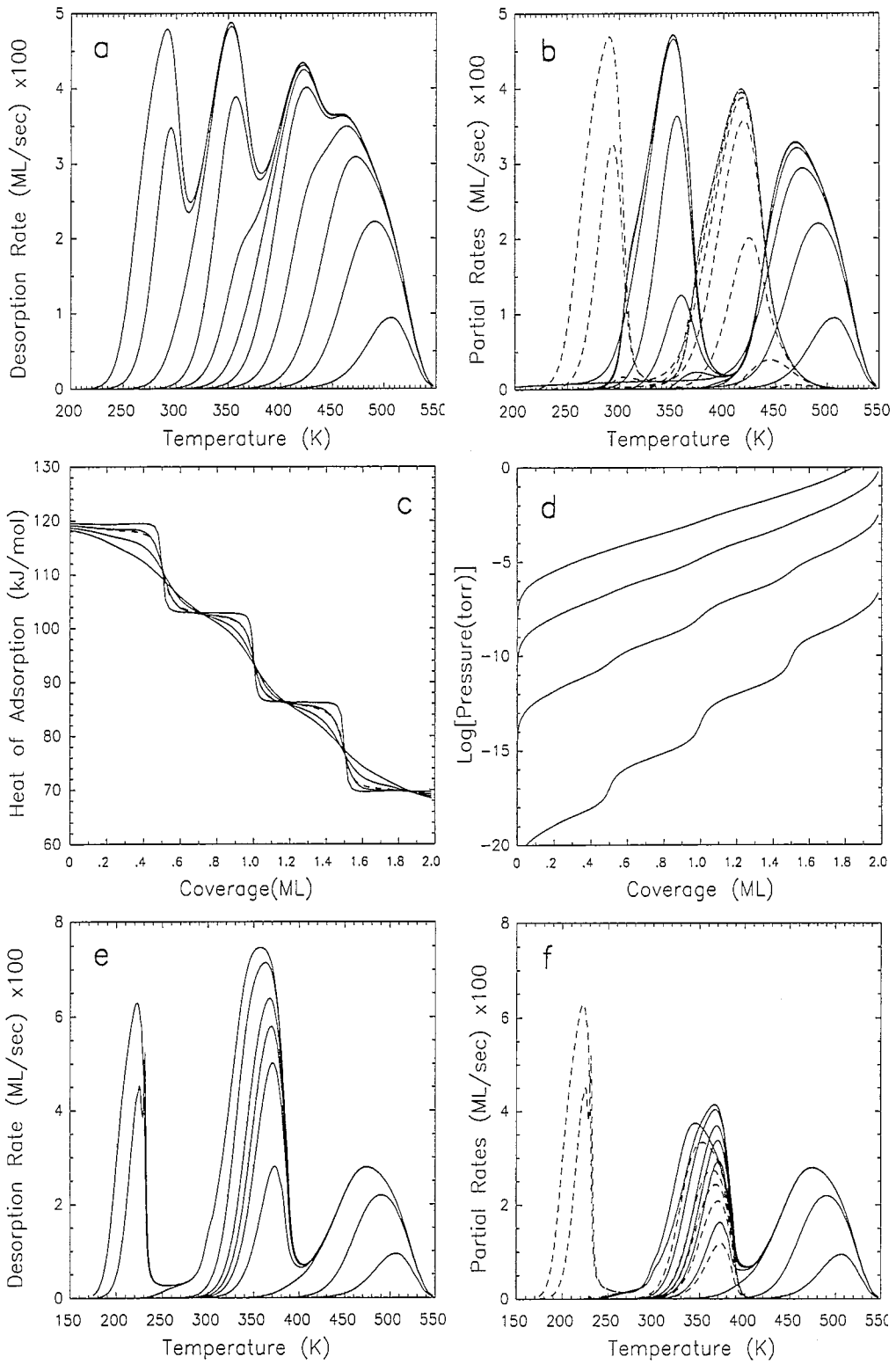

Fig. 10. Lateral repulsions in the first and second layers, $V_{11} = V_{22} = 1000$ K, $V_{12} = 0$ K. Other parameters as in Fig. 1. Two values of ΔV_0 are displayed, namely 2000 K (left column) and 4000 K (right column). (a) and (e) Total rates, initial coverages as in Fig. 1. (b) and (f) Partial rates. (c) and (g) Isothermal heat of adsorption for $T = 250$, 350, 450, 550 K (top to bottom at low θ, solid curves). Dashed curves are the temperature averaged value. (d) Pressure isotherms for the same temperatures (bottom to top) for $\Delta V_0 = 2000$ K only. (*h*) Growth curves, θ_1 (solid lines) for $T = 200$, 375, 550 K (top to bottom), and θ_2 (dashed) in reverse order for $\Delta V_0 = 2000$ K. Outer grouping (long dashed and dotted) for $\Delta V_0 = 4000$ K.

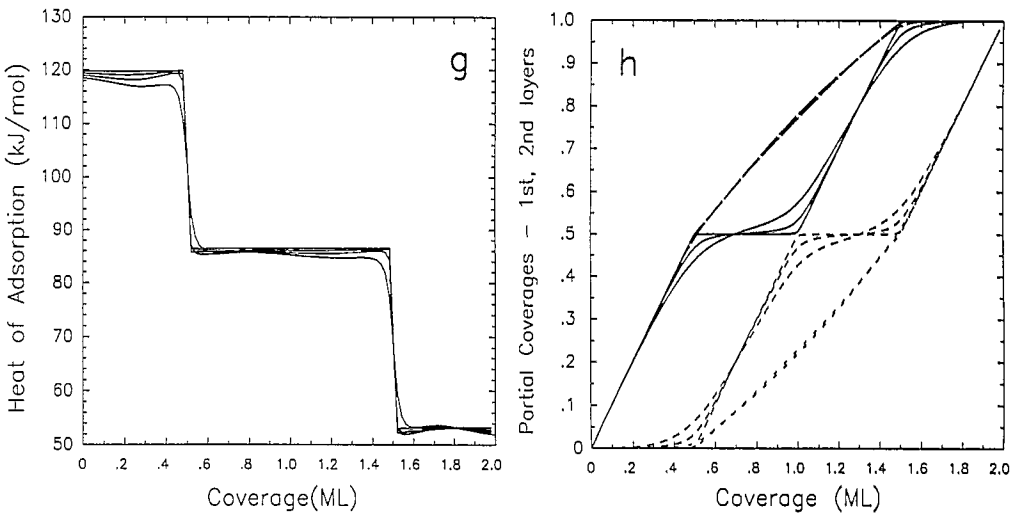

Fig. 10 (continued).

layer (isolated) results in a two peak structure then varying ΔV_0 will shift these pairs of peaks relative to each other producing apparently complex TPD spectra. The system *Cu/W*(100) [26] appears to be a candidate for repulsion in the first layer and weaker repulsion in subsequent layers.

4.5. *Next nearest neighbor / trio interactions between the layers*

In layer-by-layer growth the effect of an attractive next nearest neighbor or trio interaction, V_{12}, between the layers can clearly be subsumed into the difference in binding, ΔV_0, because each particle adsorbing in the second layer '*sees*' four next nearest neighbors below. In terms of correlation functions this implies that at completion of the first layer $\langle n_i n_j \rangle = 1$ so that $\langle n_i m_i n_j \rangle \simeq \langle n_i m_i \rangle \simeq \langle m_i \rangle$ so that the effect of V_{12} can be absorbed into E_{s2} in the Hamiltonian (1). Only at the high temperature end of the desorption range, where depopulation of the first layer occurs, can there be any departure from this fact. In dimer growth with nearest neighbor attraction in the second layer there will also not be any isolated trios at low temperature, i.e. $\langle n_i m_i n_j \rangle \simeq \langle n_i m_i n_j m_j \rangle$, so that the effect of V_{12} can be absorbed into V_{22}.

Apart from these limits it is not possible to compensate trio interactions by changing other binding or nearest neighbor interaction energies, although one might manage to produce qualitatively similar TPD spectra or equilibrium properties by some manipulations. We present results for systems where interesting effects occur which are entirely due to trio interactions.

The system of Fig. 11 has the same nearest neighbor interactions as Fig. 6 but a smaller binding difference, ΔV_0, and a repulsive trio interaction, $V_{12} = 0.5 V_{11}$. The TPD spectra are somewhat similar taking into account that the smaller binding difference moves the second layer desorption peak to higher temperatures. This difference appears in the heat of adsorption, compare Fig. 11 and Fig. 6d. In both systems the drop at half a monolayer is $4V_{11}$. In Fig. 11d this drop coincides with ΔV_0, so any deviation from a constant heat of adsorption above half a monolayer is the result of the repulsive trio interactions. This also has an effect on the growth mode in Fig. 11b. For comparison we include on this graph the growth mode in the absence of trios: because the heat of adsorption is constant above half a monolayer the probability of adsorption into the first and second layer is the same so that with twice as many second layer sites still empty, the second layer grows at twice the rate. With the trio interaction suppressing second layer growth an intermediate phase is observed for coverages between 0.5 and 0.75. Since only the attraction in the second layer can lower the energy relative to any other mode of deposition this structure must involve clusters involving both layers.

For completeness we also show the partial coverages in Fig. 11c.

If we double the trio interaction we get Fig. 12. Although the TPD spectra contains features present in both Fig. 11 and Fig. 6, the heat of adsorption most closely resembles that of Fig. 6 which exhibited layer-by-layer growth. In contrast, the growth mode is totally different. At low temperature and up to half a monolayer every second site in the first layer is occupied. Then up to $\theta = 0.75$ an intermediate phase grows as in Fig. 11c, after which the second layer particles are transferred down, due to the trio repulsion, to complete the first monolayer. The addition of one particle above a monolayer causes a large increase in the internal energy of the system (again due to the trio interaction) which is negated by a complete rearrangement of the adsorbate, namely into a 2×2 dimer structure, see Fig. 12c. Subsequent adsorption remains dimer-like due to the attraction V_{22}.

For Fig. 13 we neglect interactions in the first layer and choose a strong attraction in the second,

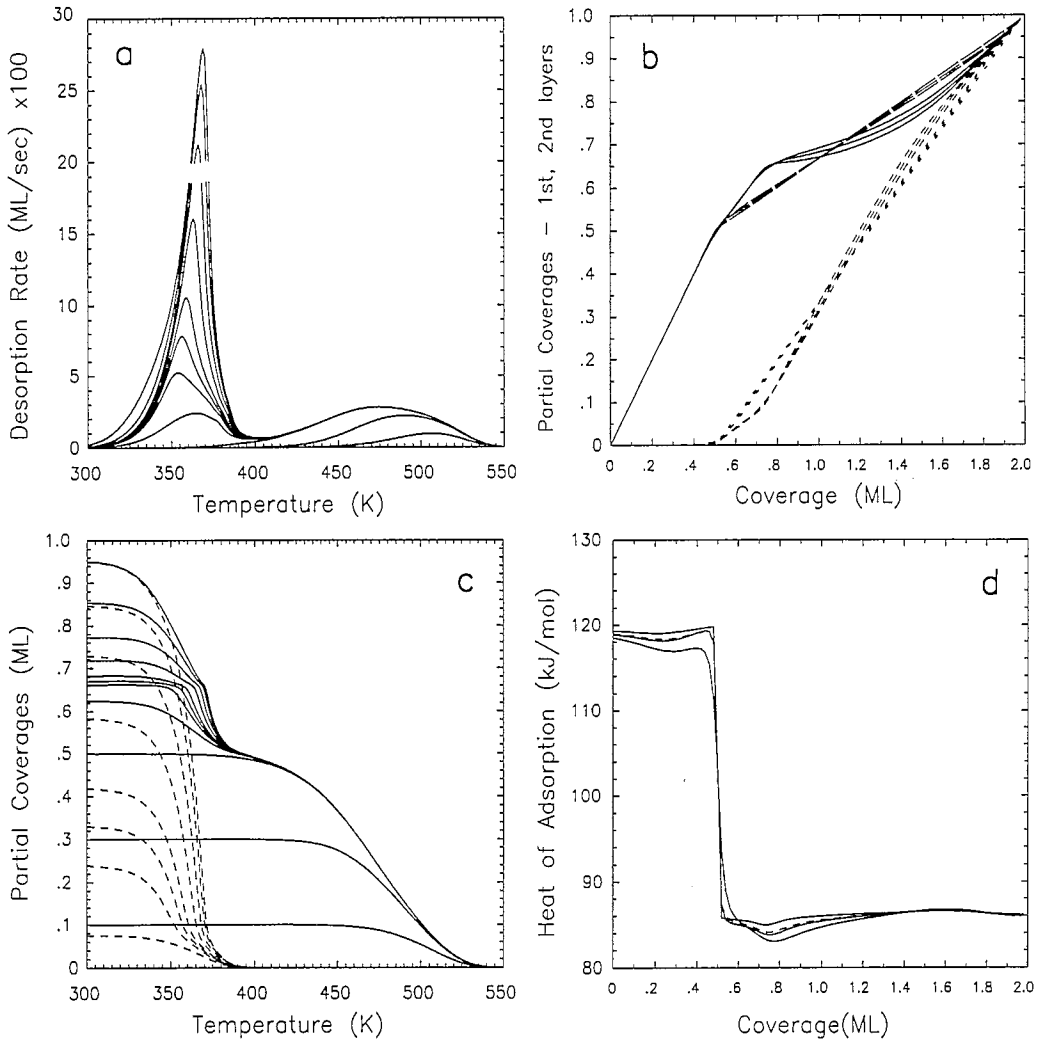

Fig. 11. Lateral repulsion in the first and attraction in the second layer, $V_{11} = -V_{22} = 1000$ K, and an interlayer trio $V_{12} = 500$ K, $\Delta V_0 = 4000$ K. Other parameters as in Fig. 1. (a) Total rates, initial coverages as in Fig. 1. (b) Growth curves, θ_1 (solid lines) for $T = 300$, 425, 550 K (bottom to top at $\theta = 1.0$), θ_2 (dashed) in reverse order. Superimposed for $V_{12} = 0$ K, θ_1 (long dashed) and θ_2 (dotted). (c) Partial coverages. (d) Isothermal heat of adsorption for $T = 300$, 400, 500 K (top to bottom at low θ, solid curves). Dashed curve is the temperature averaged value.

which favors dimer growth, and correspondingly strong trio repulsion, which will suppress dimers, which is clearly evidenced in Fig. 13b. The leading edge of the TPD spectra in Fig. 13a is due to the fact that between 1.6 and 0.8 monolayers only the second layer desorbs and from a two-phase regime. For initial coverages higher than 1.6 monolayers desorption is dimer-like. This crossover is also demonstrated in the partial coverages of Fig. 13c.

5. Summary and outlook

We have formulated a lattice gas model to deal with the adsorption and desorption kinetics in multilayer adsorbates. Its equilibrium properties are calculated using transfer matrix techniques. For adsorbates in which fast surface diffusion maintains quasi-equilibrium during adsorption and desorption we can also calculate the desorption rates essentially exactly from

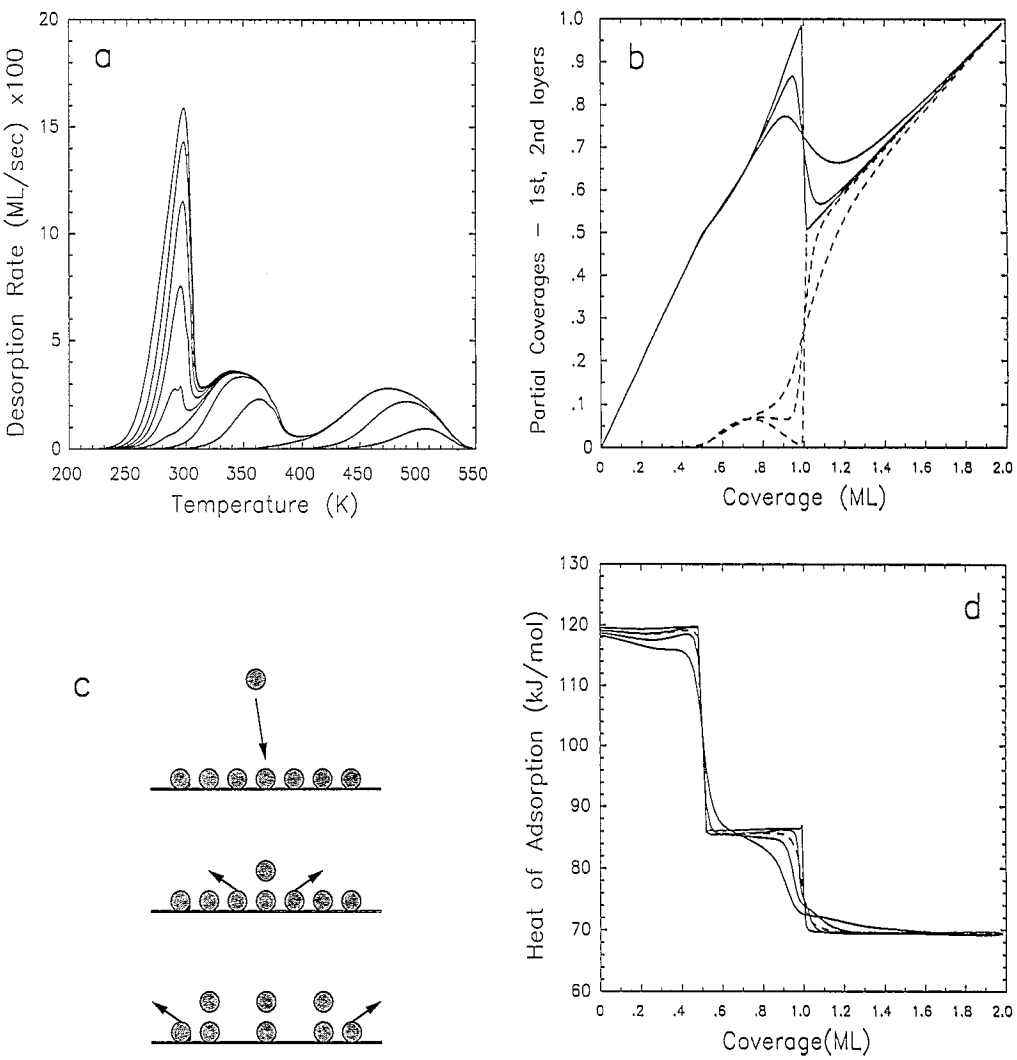

Fig. 12. As Fig. 11 but $V_{12} = 1000$ K. Other parameters as in Fig. 1. (a) Total rates, initial coverages as in Fig. 1. (b) Growth curves, θ_1 (solid lines) for $T = 250$, 400, 550 K (top to bottom at $\theta = 0.8$), θ_2 (dashed) in reverse order. (c) Schematic of the restructuring of the adsorbate at $\theta = 1.0$. (d) Isothermal heat of adsorption for $T = 250$, 350, 450, 550 K (top to bottom at low θ, solid curves). Dashed curve is the temperature averaged value.

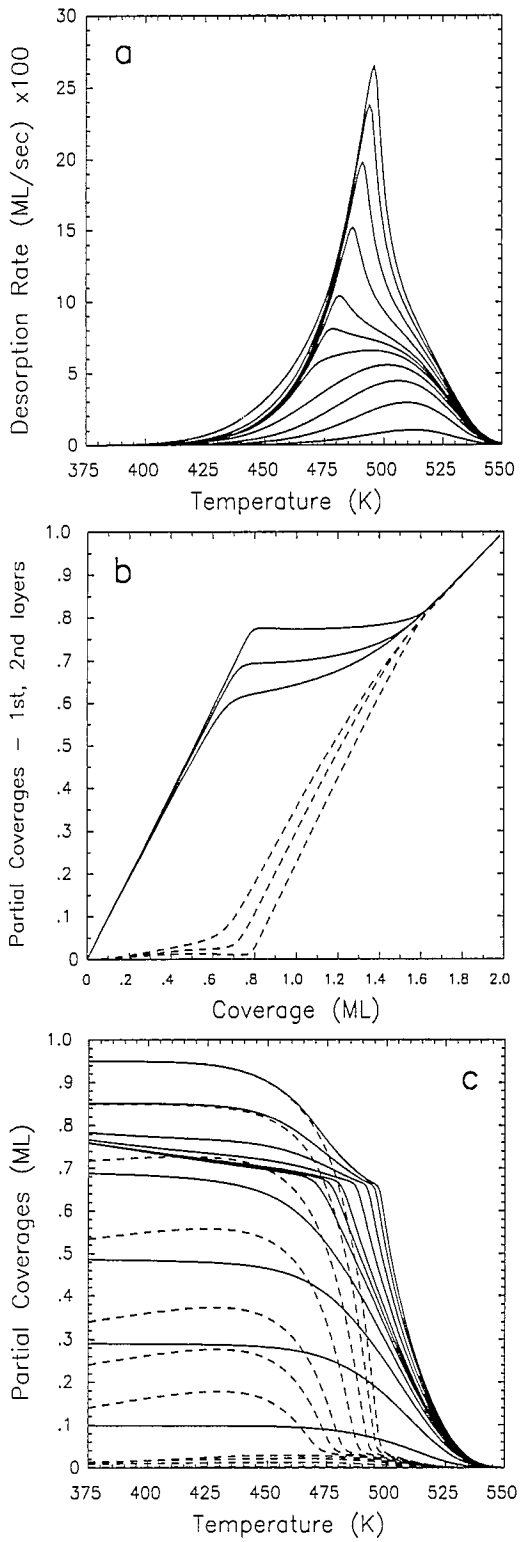

the chemical potential. Equilibrium properties, growth modes and desorption kinetics are presented for a variety of model bilayer systems. Many of the features observed in this modeling have been seen in experiments. Indeed, we will show in forthcoming papers dealing with specific systems that quantitative agreement can be obtained with data. We have emphasized throughout this paper, as we have done in our previous work, the interplay between equilibrium structures and kinetics. Neither set of data is usually sufficient to unravel the physics of the system. As an example, we point to the role of trio interactions between adjacent layers to induce structures which show up in both the growth mode and in the desorption kinetics.

The results presented in this paper are for a square lattice with on-top growth. Obviously this does not have the correct coordination for most systems for which one expects the overlayer particles to sit in bridge or hollow sites. One effect of this higher coordination will be to enhance the confinement of the lower layers. Thus many of the features of the growth modes and desorption kinetics that we have illustrated are expected to remain unchanged. The generalization of the on-top model to other lattices is straightforward and will be used in forthcoming papers dealing with particular systems. Judging from the additional complexity of the equilibrium properties and of the kinetics obtained for the hexagonal lattice in the submonolayer regime [22] we can expect interesting new features.

If surface diffusion becomes so slow that quasi-equilibrium is not maintained, we expect modifications of the growth modes and the kinetics. As an example, the *re*-organization of the adsorbate structure in the system of Fig. 12 will not occur instantaneously but the overall effect will persist. To deal properly with the interplay of surface diffusion and kinetics one avenue is the kinetic lattice gas model which has already been used to deal with submono-

Fig. 13. Non-interacting first layer, $V_{11} = 0$, attraction in second, $V_{22} = -2000$ K, and trio $V_{12} = 1000$ K with $\Delta V_0 = 500$ K. Other parameters as in Fig. 1. (a) Total rates, initial coverages as in Fig. 1. (b) Growth curves, θ_1 (solid lines) for $T = 350$, 450, 550 K (top to bottom at $\theta = 0.8$), θ_2 (dashed) in reverse order. (c) Partial coverages.

layer systems [14,30,31] and with precursor-mediated adsorption and desorption [32].

The generalization of the on-top model to multi-coordinated bonding sites is possible for a two-dimensional lattice within the transfer matrix formulation, though relatively complex compared to the present work. For a one-dimensional model we can easily deal with bridge bonded multilayers and thus examine the effect of the on-top approximation. In addition, the effects of diffusion can be examined using the kinetic lattice gas model [31].

Acknowledgements

This work was supported in part by grants from NSERC – the Natural Sciences and Engineering Research Council of Canada and from the Office of Naval Research.

References

[1] H. Schlichting and D. Menzel, Surf. Sci. 272 (1992) 27; 285 (1993) 209.
[2] E. Bauer, in: Chemical Physics of Solid Surfaces and Heterogeneous Catalysis, Vol. 3, Eds. D.A. King and D.P. Woodruff (Elsevier, Amsterdam, 1984) p. 1.
[3] M.J. de Oliviera and R.B. Griffiths, Surf. Sci. 71 (1978) 687.
[4] C. Ebner, Phys. Rev. B 28 (1983) 2890.
[5] K. Pilorz and S. Sokolowski, Z. Phys. Chemie, Leipzig 265 (1984) 929.
[6] C. Ebner, in: Chemistry and Physics of Solid Surfaces VI, Eds. R. Vanselow and R. Howe (Springer, Berlin, 1985).
[7] H. Asada, Surf. Sci. 230 (1990) 323.
[8] H. Asada and H. Sekito, Surf. Sci. 258 (1991) L697.
[9] A. Patrykiejew, S. Sokolowski, T. Zientarski and H. Asada, Surf. Sci. 314 (1994) 129.
[10] J.D. Weeks and G.H. Gilmer, Adv. Chem. Phys. 40 (1979) 157.
[11] G.H. Gilmer, in: Chemistry and Physics of Solid Surfaces V, Eds. R. Vanselow and R. Howe (Springer, Berlin, 1984).
[12] R. Kern, G. Le Lay and J.J. Metois, in: Current Topics in Materials Science, Vol.3, Ed. E. Kaldis (North-Holland, Amsterdam, 1979).
[13] E. Bauer, Appl. Phys. A 51 (1990) 71.
[14] H.J. Kreuzer and Zhang Jun, Appl. Phys. A 51 (1990) 183.
[15] H.J. Kreuzer and S.H. Payne, in: Dynamics of Gas–Surface Collisions, Eds. M.N.R. Ashfold and C.T. Rettner (Royal Soc. of Chemistry, Cambridge, 1991).
[16] C. Domb, Adv. Phys. 9 (1960) 149.
[17] F.H. Ree and D.A. Chesnut, J. Chem. Phys. 45 (1966) 3983.
[18] L.D. Roelofs and R.J. Bellon, Surf. Sci. 223 (1989) 585.
[19] N.C. Bartelt, T.L. Einstein and L.D. Roelofs, Phys. Rev. B 34 (1986) 1616.
[20] P.A. Rikvold, K. Kaski, J.D. Gunton and M.C. Yalabik, Phys. Rev. B 29 (1984) 6285.
[21] S.H. Payne, H.J. Kreuzer and L.D. Roelofs, Surf. Sci. 259 (1991) L781.
[22] S.H. Payne, Jun Zhang and H.J. Kreuzer, Surf. Sci. 264 (1992) 185.
[23] M. Paunov and E. Bauer, Appl. Phys. A 4 (1987) 201.
[24] A. Pavlovska, H. Steffen and E. Bauer, Surf. Sci. 195 (1988) 207.
[25] J.W. Niemantsverdriet, P. Dolle, K. Markert and K. Wandelt, J. Vac. Sci. Technol. A 5 (1987) 875.
[26] E. Bauer, H. Poppa, G. Todd and F. Bonczek, J. Appl. Phys. 45 (1974) 5164.
[27] S.H. Payne, H.J. Kreuzer, A. Pavlovska and E. Bauer, to be published.
[28] H. Over, H. Bludau, M. Cierer and G. Ertl, Phys. Rev. B, to be published.
[29] S.H. Payne and H.J. Kreuzer, to be published.
[30] A. Wierzbicki and H.J. Kreuzer, Surf. Sci. 257 (1991) 417.
[31] S.H. Payne, A. Wierzbicki and H.J. Kreuzer, Surf. Sci. 291 (1993) 242.
[32] H.J. Kreuzer, Surf. Sci. 231 (1990) 213.